JOURNAL OF MATERIALS SCIENCE 18 (1983) 1125–1135

Unusual stress-corrosion cracks observed in glassy Fe–40Ni–14P–6B alloy

M. D. ARCHER, R. J. McKIM
Department of Physical Chemistry, University of Cambridge, Lensfield Road, Cambridge, UK

The tendency of glassy Fe–40Ni–14P–6B to stress corrosion cracking (SCC) and hydrogen embrittlement (HE) in aqueous acidic media was investigated. Cathodically polarized, elastically stressed specimens failed in 1 M HCl by HE, as did those immersed in aqueous polythionic acid at the free corrosion potential. Similar specimens immersed in aqueous $FeCl_3$ at the free corrosion potential failed by SCC, as did those anodically polarized in 1 M HCl. The $FeCl_3$ specimens were covered with an iron oxide film, and selective leaching of nickel from pits and cracks was observed. The remarkable cracking patterns observed in aqueous $FeCl_3$ reflect the isotropic, grain -free nature of the glassy alloy surface, and are thought to throw some light upon the internal stress profile of this interesting material.

1. Introduction

Glassy ferrous-based metals are generally mechanically tough and strong, and ferromagnetically soft [1, 2]. This useful combination of properties has led to increasing interest in their commercial application to magnetic devices and tool edgings, and as claddings for conventional crystalline alloys [3, 4]. Most of these applications require that the glassy metal have good corrosion resistance in a moist environment, both to general and to localized attack.

The general corrosion behaviour of many glassy metals has been investigated [5] and it is now well established that certain additives, particularly chromium and phosphorus used together, confer excellent resistance to general corrosion on ferrous-based glasses [6, 7]. Few reports on localized corrosion have appeared: although crevice corrosion in Fe–Cr–P glasses has been induced at high potentials [8, 9], no observations of stress corrosion cracking (SCC) of glassy metals have, as far as we know, been made previously.

We have examined the susceptibility of a range of ferrous-based glassy metals to SCC and have recently reported [10] the novel SCC patterns produced in stressed Fe–40Ni–20B glass in aqueous, acidic chloride media. Here we report the even more unusual SCC patterns that we have observed in Fe–40Ni–14P–6B glass at a range of applied strains and potentials in the same media, and our speculative explanation of their uncommon form.

2. Experimental details

The melt-spun glassy alloy used (Metglas 2826, Fe–40Ni–14P–6B, where the figures indicate atomic percentages) was supplied by Allied Chemical Corporation, New Jersey, USA in the form of a 13 mm wide, 45 μm thick ribbon. One surface of the ribbon contained many small elongated depressions running parallel to the ribbon length, which had been produced by gas entrainment between ribbon and wheel during melt-spinning. The other side of the ribbon was much smoother. We shall use the terms "wheel side" and "top side" throughout to distinguish the two sides. Experiments were performed both on degreased as-received ribbons and on samples polished with Hyprez diamond paste to a 3 μm finish.

These ribbons were very springy and were elastically but not plastically deformed by coiling. SCC test specimens were prepared as described elsewhere [10, 11] by winding ribbons round

0022–2461/83 $03.00 + .12

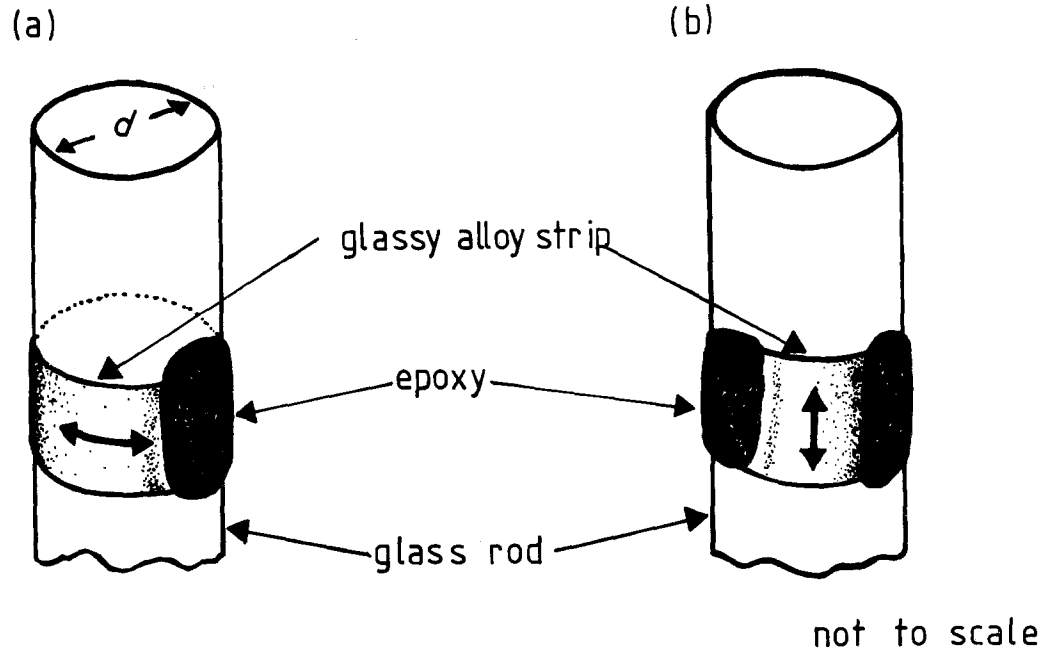

Figure 1 Experimental arrangement for stress corrosion cracking experiments. (a) transverse mounting; (b) longitudinal mounting. The long axis of the ribbon is indicated by double-headed arrows.

glass rods of diameter 3.7 to 18.4 mm. Specimens were mounted either transversely or longitudinally, as shown in Fig. 1. The applied tensile strain ϵ in the outer surface of the uncracked ribbon is given by

$$\epsilon = \frac{t}{t+d}$$

where t is the thickness of the ribbon and d is the diameter of the glass rod.

The test reagents, 0.39 M $FeCl_3$, 1 M HCl and polythionic acid [12] were prepared from AR grade reagents and distilled water. Their pHs were 1.44, 0.41 and 0.10, respectively. Solutions were open to air and thermostatted at 30° C. The $FeCl_3$ and polythionic acid tests were conducted at the free corrosion potentials. The HCl specimens were potentiostatically controlled with a Hi-Tek DT2101 potentiostat, and linear sweep voltammograms were obtained in this medium as described previously [10].

Cracked specimens were washed, dismounted and examined microscopically. High resolution work was carried out with a scanning electron microscope (SEM) with EDAX facilities. Stress corrosion behaviour was monitored as a function of time, initial applied strain and potential.

3. Results

3.1. Growth and form of cracks on ribbon side in aqueous ferric chloride

Glassy Fe–40Ni–14P–6B corrodes quite rapidly in aqueous $FeCl_3$, as the data of Table I show. SCC tests were carried out on as-received ribbon specimens which were transversely mounted top side outermost. On immersion of the SCC specimens in 0.39 M $FeCl_3$, small pits appeared on the visible surface and observable crack systems propagated from some of these pits within a few minutes. Figs. 2a to d show typical crack systems on different specimens which had been immersed for various lengths of time. The crack systems that develop at a density of 2 to 20 cm^{-2} on the

TABLE I Some corrosion data for glassy Fe–40Ni–14P–6B

Medium	Corrosion rate*	Corrosion potential†
0.39 M $FeCl_3$	1170	+ 0.15
1.00 M HCl	not measurable; < 0.3	+ 0.12
Polythionic acid	148	+ 0.09

*Units: mdd (mg dm^{-2} day^{-1}). Temperature 22° C.
†V (NHE); measured after 10 min immersion.

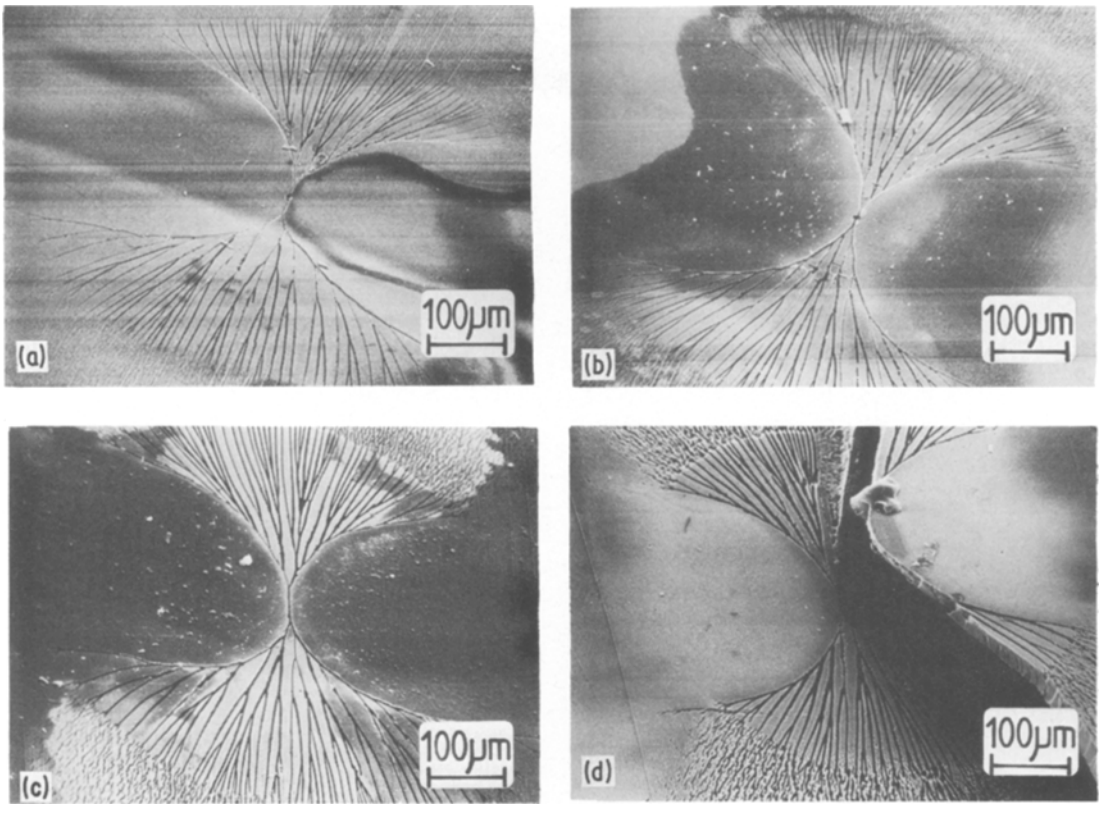

Figure 2 Scanning electron micrographs of as-received glassy Fe–40Ni–14P–6B, showing typical stress corrosion cracks formed in aerated 0.39 M $FeCl_3$ at the free corrosion potential after immersion times of (a) 5 min (b) 10 min (c) 50 min (d) 220 min. Viewing angle 45°. Applied strain $\epsilon = 0.0063$. Transversely mounted ribbon top sides exposed to solution.

outer ribbon surface show three well-defined regions labelled A, B and C in Fig. 3a. The primary region A consists of a single crack perpendicular to the applied tensile strain (i.e. parallel to the axis of the glass rod). The main crack bifurcates at each end into region B, in which several further narrow-angle bifurcations occur. Outside a well-defined boundary, a chaotic tertiary microcrack regime C, shown in close-up in Fig. 4, is observed.

In Fig. 2 (and also Figs. 4, 5 and 6) the viewing angle is 45°, which enhances contrast but distorts the appearance of the cracks. However, Fig. 3 was taken at normal incidence, which reveals the remarkably geometric form of the SCC pattern. This crack system is entirely typical, and all crack systems on this and other top side specimens were very similar. Fig. 3b illustrates crack geometry: the boundaries between regions B and C, and also between the cracked and uncracked surface, are well represented by two pairs of identical parabolae P′ and P. (The boundary between regions B and C is also well represented by an ellipse, a conic which is of course closely related to a parabola).

As the sequence of micrographs in Fig. 2 shows, a light impression of the entire crack system appears shortly after immersion. The pattern becomes more pronounced with increasing immersion time as the cracks deepen. At the same time, an observable dark brown interference film develops over the entire surface. EDAX work at 20 keV (sampling depth about 1·μm) indicated that the Fe:Ni ratio on both sides of the as-received ribbon was 1:1 The generally corroded surface was found to be about 7% depleted of nickel. Pits and cracks were much more heavily depleted of nickel. Bearing in mind that the EDAX sampling depth is considerably greater than the film thickness, these data suggest that the surface film is largely iron oxide rather than nickel oxide.

3.2. Influence of polishing and mode of ribbon mounting on crack form

The remarks of the preceding section all related

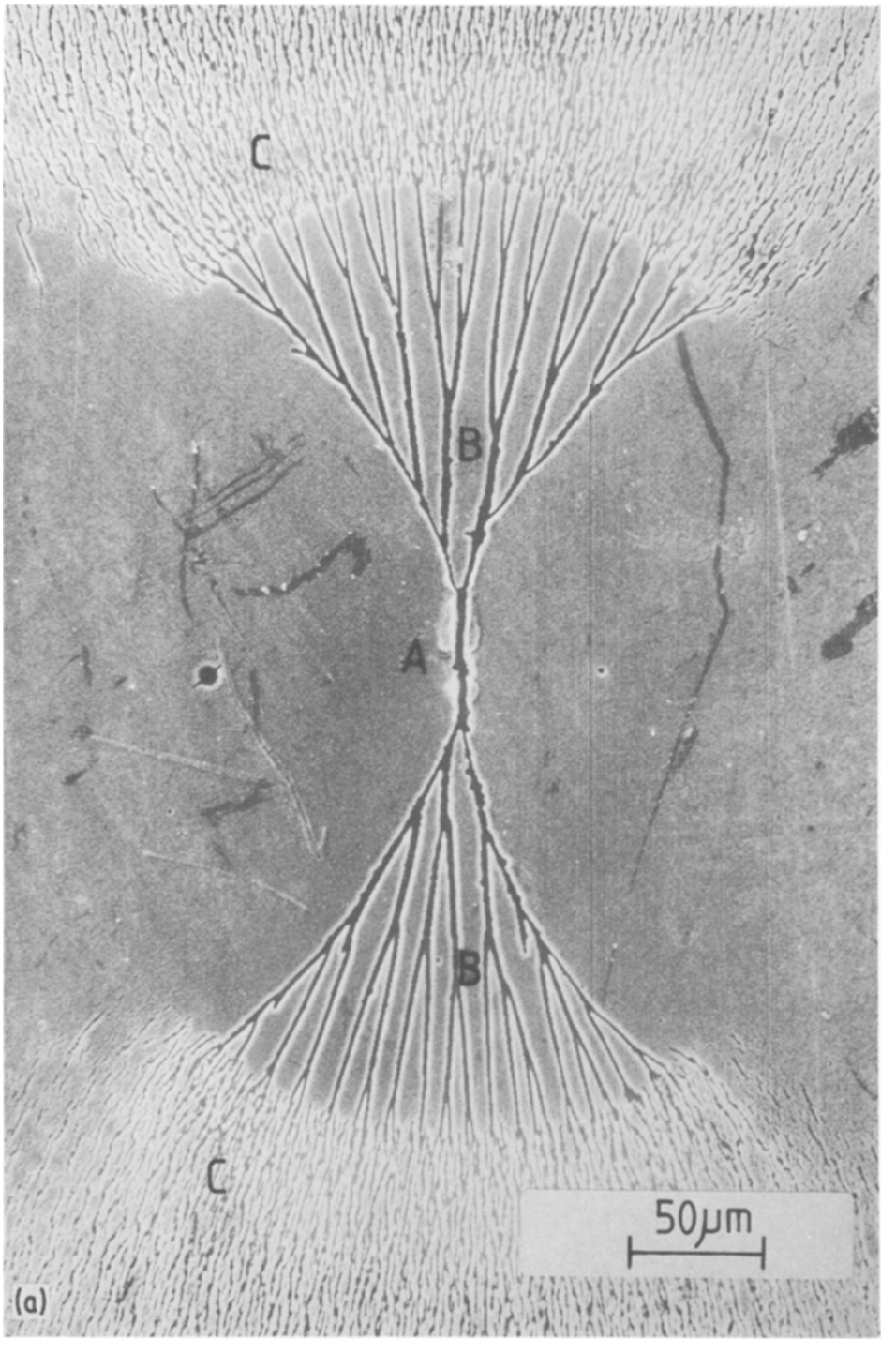

Figure 3 (a) Face-on scanning electron micrograph of typical crack system formed by 100 min immersion in 0.39 M $FeCl_3$. Tensile strain $\epsilon = 0.0063$ applied in the direction shown by the arrows. Transversely mounted ribbon top side exposed to solution. The primary, secondary and tertiary crack regions are labelled A, B and C, respectively. (b) As for (a) with parabolic overlays P and P'. The foci F and F' are also indicated.

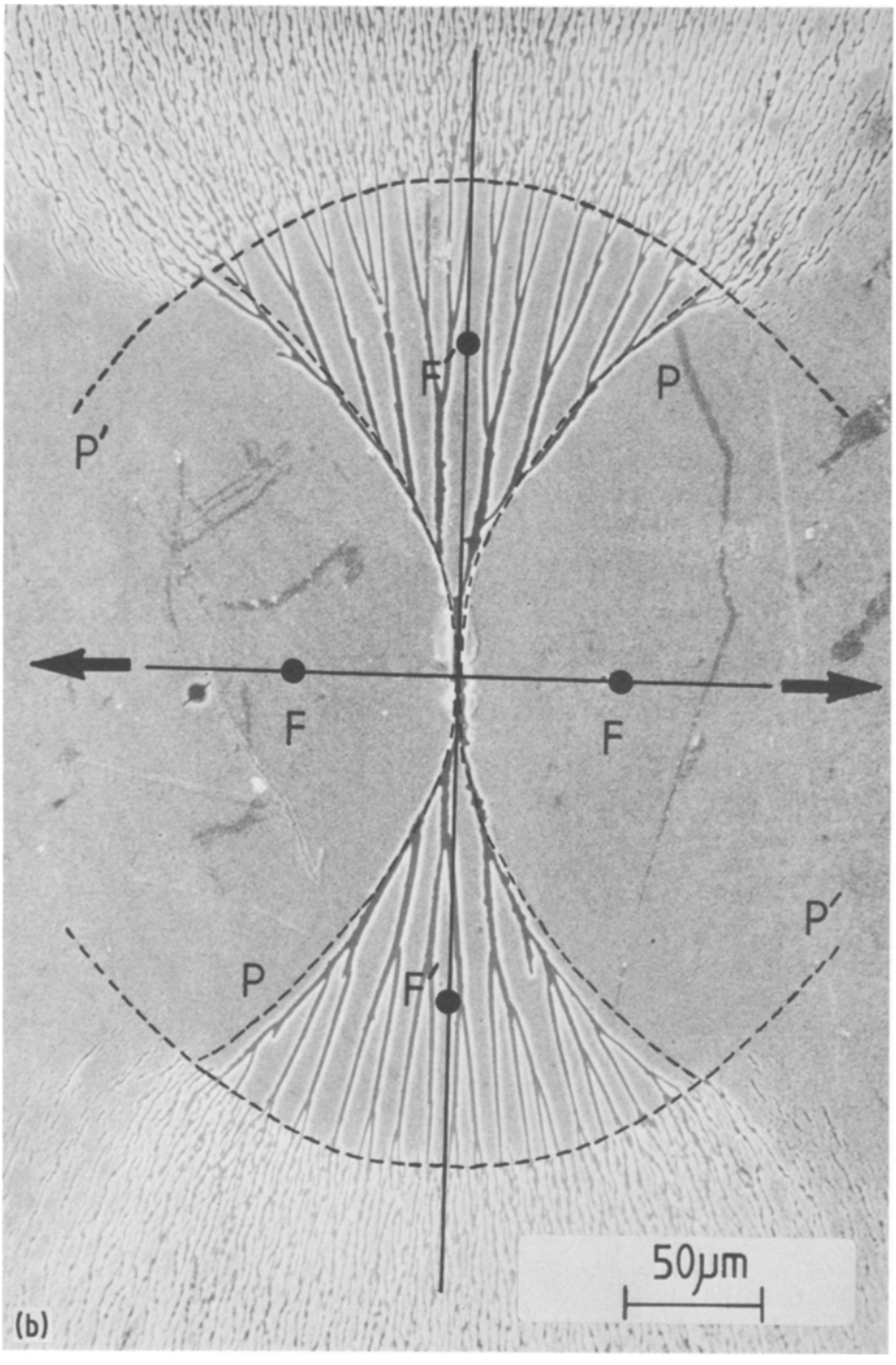

Figure 3 Continued.

to as-received specimens transversely mounted with their smooth top sides exposed to the corroding $FeCl_3$ solution. We also investigated the nature of the SCC systems formed in this medium on the much rougher wheel side of the as-received ribbons, and the effect of longitudinal mounting. Fig. 5a gives another example of the crack systems formed when the ribbon top side is transversely mounted. Fig. 5b shows, on the same scale, what happens when the wheel side is transversely

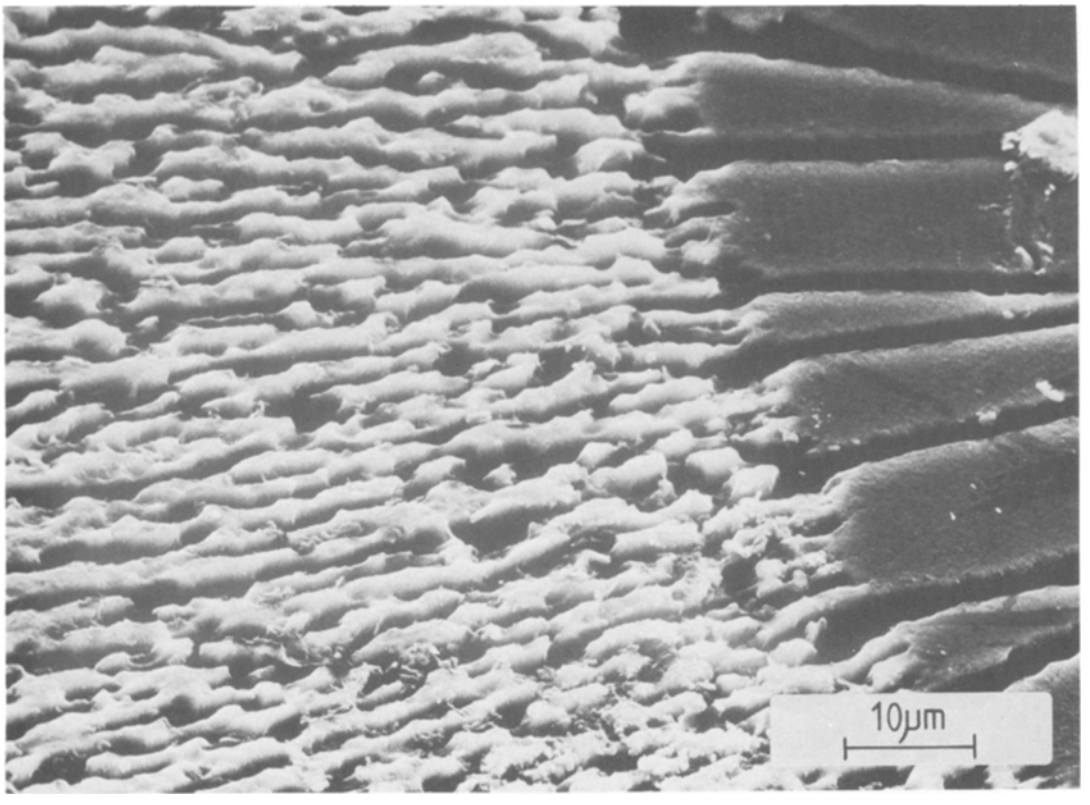

Figure 4 High-magnification micrograph of tertiary cracked region C in as-received Fe–40Ni–14P–6B. Conditions as for Fig. 2. Immersion time 105 min.

mounted: pits form preferentially in the clearly evident gas entrainment concavities. Pit density is higher, and the pits themselves are larger, than on the top side in comparable circumstances. The cracks that propagate from these wheel side pits normal to the applied stress exhibit region A as before, but region B is truncated. The tertiary microcrack regions C are much more extensive, joining up to cover the rest of the surface. The boundary between regions B and C is controlled by the surface topography.

Figs. 5c and d illustrate the effect of mounting the ribbons longitudinally. Fig. 5c is very similar to Fig. 5a, showing that the morphology of the top side cracks is unaffected by the direction of mounting. Fig. 5d, showing the cracks formed on the longitudinally mounted wheel side, is similar to Fig. 5b, except that the cracks now run parallel to the melt-spinning concavities, thereby remaining perpendicular to the applied stress.

Fig. 6 shows the effect of polishing the outer ribbon surface prior to SCC testing, on two specimens tested under identical conditions. The effects of polsihing the top side (Fig. 6a) is to generate about ten times as many crack systems per unit surface area as on the as-received material (Fig. 5a). Individual systems are therefore rather smaller, each stress-relieving a smaller area. Polishing the ribbon top sides removes large-scale gentle undulations but increases the local roughness, and this leads to higher crack density. However, each crack system is still parabolic. As Fig. 6b shows, polishing the wheel side until the gas entrainment concavities were removed produces parabolic crack systems very similar to those observed on the as-received and polished ribbon top sides.

3.3. Effect of ribbon pre-annealing

The as-received ribbons contain stresses quenched in during the melt-spinning process. These stresses can be relieved by annealing in vacuo for about 30 min at 50 K below the crystallization temperature [13]. We performed a few SCC experiments on specimens pre-annealed at 50 and 100 K below the crystallization temperature of 685 K [14]. The annealed specimens were rather brittle, but could usually be wound on to glass

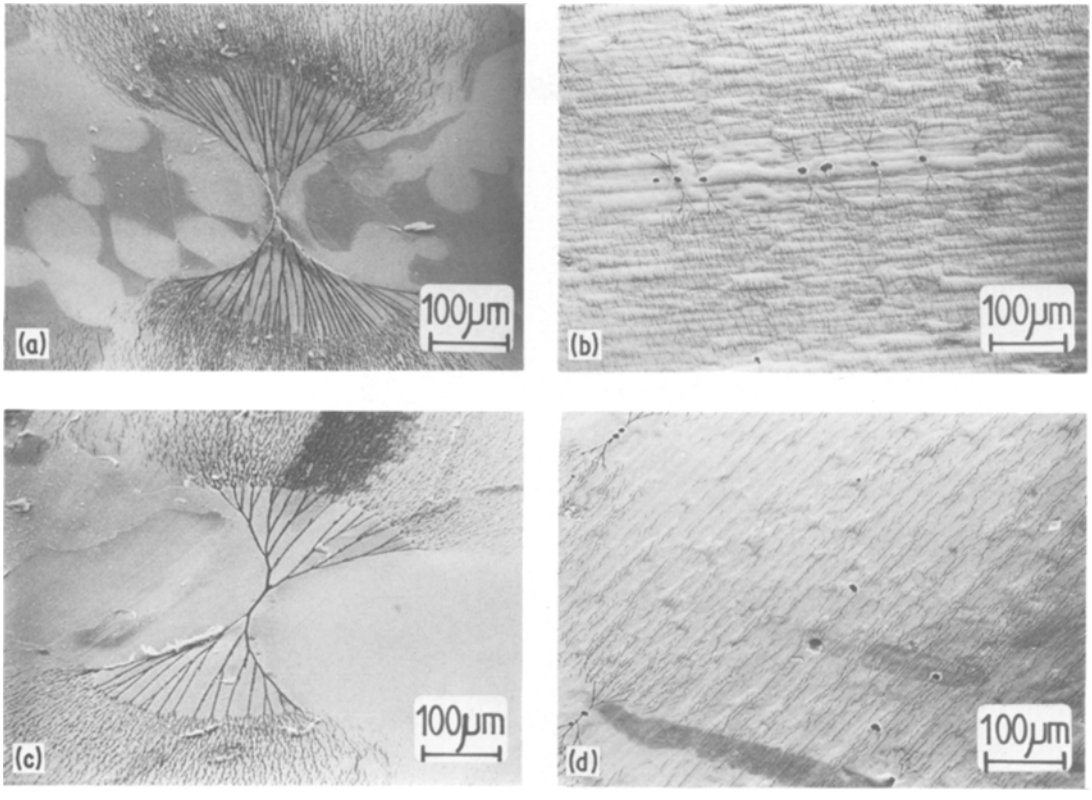

Figure 5 Illustration of effect of ribbon mounting mode. (a) Top side transverse; (b) wheel side transverse; (c) top side longitudinal; (d) wheel side longitudinal. Conditions as for Fig. 2. Immersion time 100 min.

rods without snapping immediately, although some failed overnight in moist air. However, annealed specimens immersed in $FeCl_3$ failed catastrophically within a few seconds by the rapid propagation of a single crack across the entire ribbon width. Thus annealing embrittles the specimens so severely that the normal SCC pattern is not observed.

3.4. Effect of applied strain

The crack systems on stressed specimens in aqueous $FeCl_3$ deepened with immersion time as illustrated in Fig. 2. Eventually, the samples failed catastrophically, springing off the rod, and fracturing around and between individual crack systems. Fig. 2d shows a partially failed sample, in which one of the outer crack envelopes has penetrated right

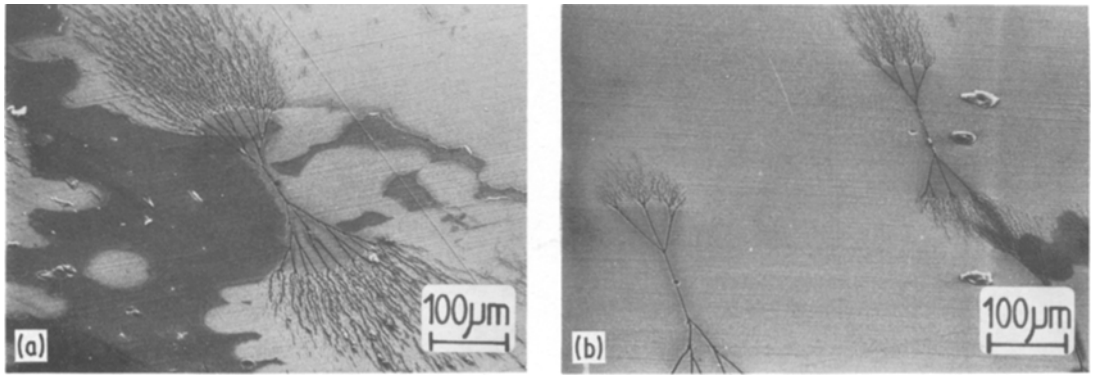

Figure 6 Illustration of effect of polishing. (a) polished top side transverse; (b) polished wheel side transverse.

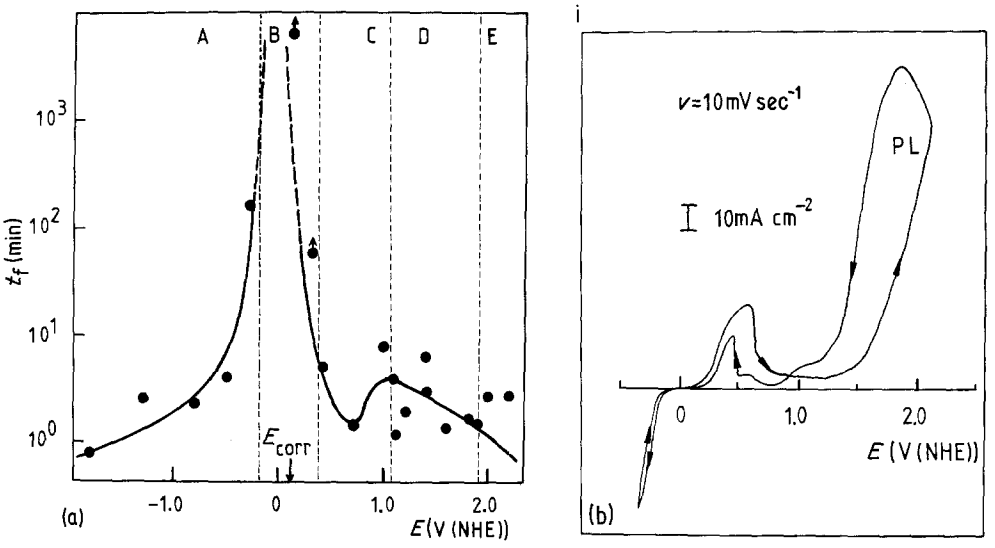

Figure 7 (a) Time-to-failure t_f of as-received transversely mounted glassy Fe–40Ni–14P–6B in 1 M HCl as a function of potential E. Initial strain $\epsilon = 0.0063$. A, B, C, D and E denote regions described in the text. E_{corr}, the free corrosion potential is indicated. (b) Linear sweep voltammogram in 1 M HCl. Sweep rate v and the pitting loop PL are indicated. Temperature 23° C.

through the ribbon. In a catastrophically failed sample, these crack envelopes are joined by irregular cracks through the tertiary regions. Experiments on the as-received material showed that there was only a slight dependence of the time to catastrophic failure on initial applied strain. Lightly stressed ($\epsilon \sim 0.003$) specimens took a little longer to fail, but exhibited SCC patterns similar to those of heavily stressed ($\epsilon \sim 0.012$) specimens. Lightly stressed specimens had fewer, but larger, cracks on their failed surfaces. The tertiary microcrack region C was barely evident on lightly stressed specimens, but very extensive on heavily stressed specimens. Unlike the Fe–40Ni–20B glassy alloy which we have previously investigated in the same medium [10], there was no threshold strain below which cracking did not occur.

3.5. Potential dependence of time to failure in aqueous hydrochloric acid

The free corrosion potential of glassy Fe–40Ni–14P–6B in 1 M HCl is lower than in 0.39 M $FeCl_3$, and the weight loss in HCl is undetectable (see Table I). We investigated the behaviour of samples potentiostatically controlled in 1 M HCl. Fig. 7a shows the time of catastrophic failure t_f of as-received specimens transversely mounted in 1 M HCl as a function of potential E. Ribbon top sides were exposed to the solution.

Five zones of behaviour are demarcated in Fig. 7a. Cathodized samples (region A) failed abruptly by hydrogen embrittlement. The fracture surfaces consisted of locally rough and smooth areas, but we did not observe any Wallner lines on them. Hydrogen embrittlement of glassy Fe–40Ni–14P–6B has also been reported by others [15]. The time to failure t_f decreased with increasing cathodic overpotential, indicating that hydrogen uptake (and consequent embrittlement) was tending to a limit. Around the free corrosion potential (region B), the specimens corroded away slowly, and no significant cracking was observed. In a narrow zone (region C) just anodic of the free corrosion potential, crack systems and oxide films identical to those produced by $FeCl_3$ were formed. Still higher potentials (region D) produced rather longer cracks with a different branching pattern [16]. No brown films had formed on the surfaces of these specimens before they failed catastrophically. Very high anodic potentials (> 1.9 V (NHE), region E) yielded darkened surfaces marked by many tiny pits and cracks, and rapid sample failure occurred by crevice corrosion at the interfaces between the ribbon and the epoxy seals.

Fig. 7b shows the linear sweep voltammogram of the glassy alloy in 1 M HCl. A comparison of Figs. 7a and b shows that the time to failure at potentials anodic to the free corrosion potential is inversely related to the current density, an unsurprising result. A small active-passive transition

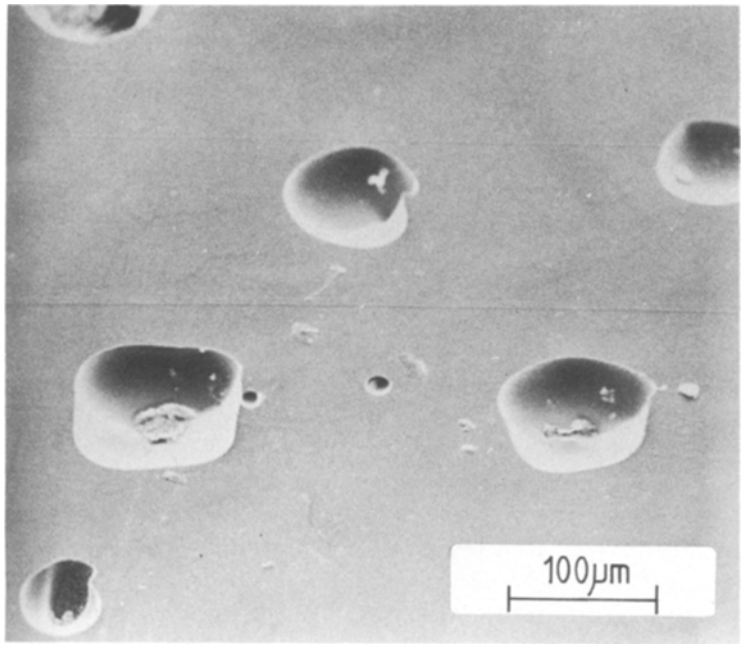

Figure 8 Micrograph of pits formed in top side of as-received Fe–40Ni–14P–6B by potential cycling between −0.36 and 2.12 V (NHE) in 1 M HCl. Viewing angle 45°. The debris in the pits is silver dag from the SEM mount.

is evident in Fig. 7b. The passive region is short, and the marked pitting loop PL confirms the occurrence of localized attack. Larger pits can be grown by potential cycling of the unstressed materials in 1 M HCl, as Fig. 8 illustrates.

3.6. Behaviour in aqueous polythionic acid

Stressed specimens immersed in aqueous polythionic acid failed by hydrogen embrittlement. The surface of the alloy darkened rapidly during testing, becoming dark and lustrous. No stress corrosion cracking occurred: rather, the surface of the alloy appeared to buckle in places. The ribbon then failed sharply by the rapid propagation of a single brittle crack across the sample width. Microscopy did not yield anything very informative. There was an apparent association of (elemental?) sulphur with the cracks. The time to failure did not depend strongly upon the applied strain. All samples examined over the range $\epsilon = 0.003$ to 0.012 failed in the same way. The free corrosion potential of the glassy alloy in polythionic acid (see Table I) is rather lower than in $FeCl_3$ or HCl, so the occurrence of HE in preference to SCC is not surprising. The corrosion rate of Fe–40Ni–14P–6B in this medium, while much lower than that in $FeCl_3$, is still quite appreciable.

4. Discussion

Hydrogen embrittlement of glassy Fe–40Ni–14P–6B, both on cathodic polarization in 1 M HCl and at the free corrosion potential in aqueous polythionic acid, was not unexpected. Such behaviour has been reported by others [11, 15]. We have also observed HE of glassy Fe–40Ni–20B [10]. Glassy alloys are very strong materials [2] and their suscepibility to HE is similar to that of high-strength crystalline steels.

In acidic chloride-containing media, stress corrosion cracking is observed. The active-passive transition of Fig. 7b indicates that the classic conditions for SCC are met. The form of the crack systems on $FeCl_3$ specimens is remarkable, and quite unlike anything observed in crystalline alloys, in which the local grain structure leads to zig-zag SCC patterns that can be transgranular or intergranular [17]. The primary crack region A (Fig. 3a) consists of a single crack which propagates from a generally obvious central pit. Subsequent bifurcation into region B is probably caused by the shear stress which builds up at the crack tip as the crack propagates normal to the applied tensile strain. The further behaviour is not so readily accounted for. In glassy Fe–40Ni–20B [10] the SCC pattern, although again reflecting the lack of grain structure, is much less complex. A small change in the chemical composition of the alloy

has seemingly had a marked effect upon crack morphology. We believe, however, that the explanation of the elaborate SCC patterns observed on Fe–40Ni–14P–6B is not purely chemical.

The internal tensile properties of the glassy metal may partly account for the observed crack behaviour, and we draw here a speculative analogy with toughened silicate glass. Silicate glass can be thermally toughened by rapid quenching from the melt. During cooling, the surfaces solidify before the interior. In consequence, the outer portion of the cooled glass is under compressive stress while the interior is under tensile stress [18]. If a surface flaw penetrates through the compressed surface layer to the inner tensile region, crack propagation will occur even in the absence of any externally applied strain. Such conditions cause a penetrating crack to accelerate and branch. The biaxial nature of the internal tensile stress allows crack propagation in any plane perpendicular to the surface. Hence both branches of the initial crack will propagate and will themselves branch. Melt-spinning of glassy metals involves very high cooling rates, and both sides of the ribbon must necessarily cool more quickly than the interior. Consequently, an internal stress profile similar to that of toughened silicate glass may well be produced. If such a stress profile existed in glassy Fe–40Ni–14P–6B, it would explain the escalation of crack branching once an initiating pit has entered the inner region of tensile stress. It is notable that the width (13 mm) of Fe–40Ni–14P–6B is greater than that of the Fe–40Ni–20B (3 mm) which we investigated previously [10]: perhaps the internal tensile stress is higher in the wider ribbon. The SCC cracking patterns on polished specimens or on the as-received ribbon top side are independent of whether the specimens are mounted transversely or longitudinally: this is consistent with our hypothesis of biaxial internal tensile stress. The wheel side cracks (Figs. 5b and d) are strongly influenced by the roughness of this surface. However, when this side is polished (Fig. 6b), the characteristic parabolic behaviour emerges.

The parabolic perfection of the $FeCl_3$ crack systems (Fig. 3) invites a mathematician's attention. While the shape is qualitatively explicable in terms of the applied stress produced by bending the ribbon combined with the proposed internal biaxial stress, a quantitative treatment of the fracture mechanics would be extremely difficult. Experiments on ribbons in plane strain should be easier to interpret.

Despite the possibility that cracking patterns are influenced by the internal stress profile of the ribbon, the considerable variations in crack form with applied potential, and the selective leaching of nickel from the sites of localized attack, show that chemical effects are also important. Strain dependence of SCC is readily explained. At high ϵ, many pits on the surface of the alloy are able to propagate into cracks, so each crack system is is required to strain-relieve only a small area of surface. At lower ϵ, fewer pits propagate into crack systems, so each is considerably larger. The variation of the crack morphology of Fe–40Ni–14P–6B in 1 M HCl with applied potential is complicated [16], but certainly reflects the tendency to passivate at each potential. Ferric chloride-like cracks are produced in a narrow region of potential anodic with respect to the free corrosion potential. Pitting also occurs in the "passive" region. Chloride ions have a deleterious effect on the ability of this glassy alloy to passivate, as they do for crystalline ferrous-based alloys. The baser glassy alloy Fe–40Ni–20B does not passivate in 1 M HCl [10].

Investigations into the SCC susceptibility of a wide range of commerically available and home-made glassy alloys are in progress [19].

5. Conclusions

Fe–40Ni–14P–6B, in common with certain other ferrous-based glassy metals, is susceptible to both HE and SCC. The unusual form of the stress corrosion cracks produced in acidic chloride-containing media may be influenced by the internal tensile properties of the alloy. Potential dependence of crack morphology indicates, however, that chemical effects cannot be ignored. Glassy alloys have no grain structure, and the reproducible forms of their stress corrosion cracks make them interesting subjects for investigation.

Acknowledgements

We thank Dr J. F. Knott of the Department of Metallurgy, Cambridge University, for helpful discussions, and SERC for financial support.

References

1. P. CHAUDHARI, B. C. GIESSEN and D. TURNBULL, *Sci. Amer.* **242(4)** (1980) 98.
2. T. MASUMOTO and R. MADDIN, *Mat. Sci. Eng.* **19** (1975) 1.

3. C. GRANT and R. McKIM, *New Sci.* **94** (1982) 637.
4. P. DUWEZ, *Proc. Indian Acad. Sci.* C2 (1979) 117.
5. Y. WASEDA and K. T. AUST, *J. Mater. Sci.* **16** (1981) 2337.
6. M. NAKA, K. HASHIMOTO and T. MASUMOTO, *J. Non-Crystalline Sol.* **28** (1978) 403.
7. D. R. BAER and M. T. THOMAS, *J. Vac. Sci. Technol.* **18** (1981) 722.
8. T. M. DEVINE, *J. Electrochem. Soc.* **134** (1977) 38.
9. R. B. DIEGLE, *Corrosion* **36** (1980) 362.
10. M. D. ARCHER and R. J. McKIM, *ibid.* in press.
11. A. KAWASHIMA, K. HASHIMOTO and T. MASUMOTO, *ibid.* **36** (1980) 577.
12. ASTM Standard Recommended Practice, Designation: G35-73 (1973).
13. T. EGAMI, *J. Mater. Sci.* **13** (1978) 2587.
14. Metglas Technical Literature.
15. J. T. WANG, Q. H. SONG and S. L. LI, in "Proceedings of the 4th International Conference on Rapidly Quenched Metals" Vol. 2, edited by T. Masumoto and K. Suzuki (Japanese Institute of Metals, Sendai, Japan, 1982) p. 1625.
16. R. J. McKIM, PhD dissertation, Cambridge University (1983), gives micrographs of the varied cracking patterns observed in 1 M HCl as a function of potential.
17. A. J. SEDRIKS, "Corrosion of Stainless Steels" (Wiley, New York, 1979).
18. D. G. HOLLOWAY, "The Physical Properties of Glass" (Wykeham, London, 1973).
19. R. J. McKIM and M. D. ARCHER, unpublished work (1982).

Received 19 August
and accepted 6 September 1982